

Deep neural networks for solving forward and inverse problems of (2+1)-dimensional nonlinear wave equations with rational solitons

Zijian Zhou^{1,2}, Li Wang^{3,4}, and Zhenya Yan^{1,2,*}

¹*Key Laboratory of Mathematics Mechanization, Academy of Mathematics and Systems Science, Chinese Academy of Sciences, Beijing 100190, China*

²*School of Mathematical Sciences, University of Chinese Academy of Sciences, Beijing 100049, China*

³*Yanqi Lake Beijing Institute of Mathematical Sciences and Applications, Beijing, 101408, China*

⁴*Yau Mathematical Sciences Center and Department of Mathematics, Tsinghua University, Beijing, 100084, China*

Abstract. In this paper, we investigate the forward problems on the data-driven rational solitons for the (2+1)-dimensional KP-I equation and spin-nonlinear Schrödinger (spin-NLS) equation via the deep neural networks leaning. Moreover, the inverse problems of the (2+1)-dimensional KP-I equation and spin-NLS equation are studied via deep learning. The main idea of the data-driven forward and inverse problems is to use the deep neural networks with the activation function to approximate the solutions of the considered (2+1)-dimensional nonlinear wave equations by optimizing the chosen loss functions related to the considered nonlinear wave equations.

Keywords: (2+1)-dimension nonlinear wave equations; deep neural networks learning; activation function; data-driven rational solitons; data-driven parameter discovery

1 Introduction

In the past decade, data analysis and machine learning with neural networks have been paid more attention to and achieved some significant advances due to the explosive development of big data and computing resources. As a result, these progresses further promoted the rapid development of other related fields, including computer vision, natural language processing, cognitive science, optical text/character recognition and data assimilation [1–6], etc.. Hornik *et al* showed that the standard multi-layer feedforward networks with one hidden layer and arbitrary bounded and nonconstant activation function could approximate any Borel measurable function in any accuracy if the sufficiently many hidden units are available [7,8]. And the other some works provided some new perspectives on the functions of the neural networks (see, e.g., Refs. [9–12] and references therein). The main idea of deep neural networks learning is to use the simple compositions of linear functions and nonlinear activation functions to represent the solved functions. Some recent studies have focused on the applications of deep learning in the high-dimensional problems, including the partial differential equations (PDEs) [13, 14], stochastic differential equations (SDEs) [15, 16] and molecular dynamics [17, 18].

In recent years, many deep neural networks focused on the study of differential equations, such as the physics-informed neural networks (PINNs) [20–23], deep Ritz method [19], deep Galerkin method (DGM) [24], PDE-net [25, 26], and etc. The physical constraints are added to the loss functions to powerfully learn the models [20]. In Refs. [19, 21], the equation loss was replaced by the variational loss. In addition, many other works extended these deep neural networks learning methods solving the PDEs (see, e.g., Refs. [27–35]).

In this work, we would like to investigate the following forward and inverse problems of high-dimensional nonlinear wave equations via the deep learning method. We consider these problems in $(\mathbf{x}, t) \in D \times [t_0, t_1] \in \mathbb{R}^{n+1}$.

**Email address:* zyyan@mmsrc.iss.ac.cn (Corresponding author)

- Forward problem: For the given higher-dimensional nonlinear equation ($F(q, q_x, q_t, \dots) = 0$) with the initial data ($q(\mathbf{x}, 0) = q_0(\mathbf{x})$) and periodic boundary conditions

$$\begin{cases} F(q, q_x, q_t, \dots) = 0, \\ q(\mathbf{x}, t_0) = q_0(\mathbf{x}), & \mathbf{x} \in D, \quad \mathbf{x}_{B_1}, \mathbf{x}_{B_2} \in \partial D, \quad t \in [t_0, t_1] \\ q(\mathbf{x}_{B_1}, t) = q(\mathbf{x}_{B_2}, t), \end{cases} \quad (1)$$

one would like to use the deep learning method to emulate the data-driven solution $q(\mathbf{x}, t)$ of Eq. (1).

- Inverse problem: For the given solution data ($q_0(\mathbf{x}, t)$), one would like to use the deep learning method to discover the unknown parameters $\mathbf{p} \in \mathbb{R}^m$ of $F(\mathbf{p}, q, q_x, q_t, \dots) = 0$ by considering

$$\begin{cases} F(\mathbf{p}, q, q_x, q_t, \dots) = 0, \\ q(\mathbf{x}, t) = q_0(\mathbf{x}, t), \end{cases} \quad \mathbf{x} \in D, \quad t \in [t_0, t_1], \quad \mathbf{p} \in \mathbb{R}^m. \quad (2)$$

where $\mathbf{x} = (x_1, x_2, \dots, x_n)$ and $\mathbf{p} = (p_1, p_2, \dots, p_m)$.

The rest of this paper is arranged as follows. In Sec. 2, we simply introduce the PINN scheme for the forward problem, and study the data-driven rational solitons of the (2+1)-dimensional KP-I equation and spin-NLS equation via the PINN deep learning. In Sec. 3, we introduce the PINNs scheme for the inverse problem, and apply it to discover the parameters of the associated functions in the (2+1)-D KP-I equation and spin-NLS equation. Finally, we give some conclusions and discussions in Sec. 4.

2 Forward problems in high-dimensional nonlinear wave equations

2.1 The deep neural networks learning scheme

In this subsection, we would like to briefly introduce the PINN deep learning method [20] for the forward problem (see the data-driven solutions of Eq. (1)) in the high-dimensional space. It is well-known that the curse of dimensionality is a big problem in usual numerical algorithms, but the high-dimensional problem is not a big deal for the deep learning method. The main idea of the PINN method is to use a deep neural network to fit the solutions of Eq. (1). The number of input neuron denotes the number of variable. Fig. (1) depicts the structure of the PINN method for forward problem in (2 + 1)- D case. Next, we will describe its structure in detail. For convenience, we illustrate the method in (2+1)-D case, and just discuss the periodic boundary conditions. In fact, other kinds of boundary conditions can also be considered in the same way.

We assume that $q(\mathbf{x}, t)$ is a solution of $F(q, q_x, q_t, \dots) = 0$. Let $q(\mathbf{x}, t) = u(\mathbf{x}, t) + iv(\mathbf{x}, t)$ with $u(\mathbf{x}, t)$, $v(\mathbf{x}, t)$ being its real and imaginary parts, and \mathbf{x} represent the spatial variable (i.e. $\mathbf{x} = (x_1, x_2)$). The complex-valued function $F(q, q_x, q_t, \dots)$ can be written as $F(q, q_x, q_t, \dots) = F_u(q, q_x, q_t, \dots) + iF_v(q, q_x, q_t, \dots)$ with $F_u(q, q_x, q_t, \dots)$, $F_v(q, q_x, q_t, \dots)$ being its real and imaginary parts, respectively. We will approximate the solution $q(\mathbf{x}, t)$ by using a complex-valued deep neural network $\hat{q}(\mathbf{x}, t) = (\hat{u}(\mathbf{x}, t), \hat{v}(\mathbf{x}, t))$ written as

```
def q(x1, x2, t):
    q = neural_net(tf.concat([x1, x2, t], 1), weights, biases)
    u = q[:, 0:1]
    v = q[:, 1:2]
    return u, v
```

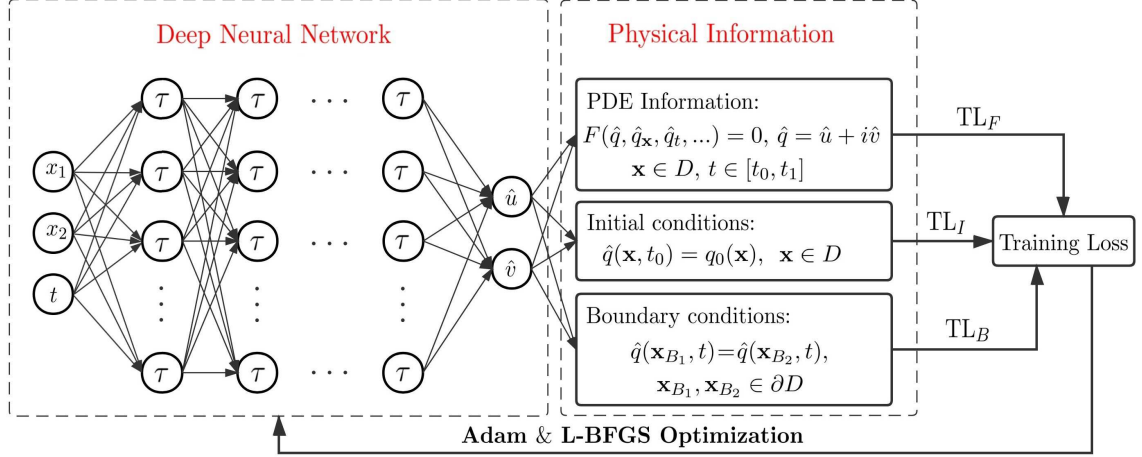


Figure 1: The PINN scheme solving the forward problem (1), where \mathcal{T} denotes the activation function (e.g., $\mathcal{T} = \tanh(\cdot)$).

Based on the defined function $q(\mathbf{x}, t)$, the physics-informed neural network $F(q, q_x, q_t, \dots)$ can be taken as

```
def F(x1, x2, t):
    u, v = q(x1, x2, t)
    u_t = tf.gradients(u, t)[0]
    u_x1 = tf.gradients(u, x1)[0]
    u_x2 = tf.gradients(u, x2)[0]
    ...
    v_t = tf.gradients(v, t)[0]
    v_x1 = tf.gradients(v, x1)[0]
    v_x2 = tf.gradients(v, x2)[0]
    ...
    F_u = (real part of F(q, q_x, q_t, ...))
    F_v = (imaginary part of F(q, q_x, q_t, ...))
    return F_u, F_v
```

where $\hat{q}(\mathbf{x}, t) = \hat{u}(\mathbf{x}, t) + i\hat{v}(\mathbf{x}, t)$ and $F(q, q_x, q_t, \dots) = F_u(q, q_x, q_t, \dots) + iF_v(q, q_x, q_t, \dots)$ share the same parameters, weights and biases, and the deep neural network can be learned by optimizing the training loss (TL). In the forward problem (1), the training loss (TL) is assumed as the sum of three parts including the initial loss (TL_I), the boundary loss (TL_B), and the equation loss (TL_F):

$$TL = TL_I + TL_B + TL_F, \quad (3)$$

where the three parts of loss are defined by the mean squared errors (i.e., \mathbb{L}^2 -norm):

$$\begin{aligned}\text{TL}_I &= \frac{1}{N_I} \sum_{j=1}^{N_I} \left[\left(\hat{u}(\mathbf{x}_I^j, t_0) - u(\mathbf{x}_I^j, t_0) \right)^2 + \left(\hat{v}(\mathbf{x}_I^j, t_0) - v(\mathbf{x}_I^j, t_0) \right)^2 \right], \\ \text{TL}_B &= \frac{1}{N_B} \sum_{j=1}^{N_B} \left[\left(\hat{u}(\mathbf{x}_{B_1}^j, t_B^j) - \hat{u}(\mathbf{x}_{B_2}^j, t_B^j) \right)^2 + \left(\hat{v}(\mathbf{x}_{B_1}^j, t_B^j) - \hat{v}(\mathbf{x}_{B_2}^j, t_B^j) \right)^2 \right], \\ \text{TL}_F &= \frac{1}{N_F} \sum_{j=1}^{N_F} \left(F_u^2(\mathbf{x}_F^j, t_F^j) + F_v^2(\mathbf{x}_F^j, t_F^j) \right),\end{aligned}\tag{4}$$

with $\{\mathbf{x}_I^j, u(\mathbf{x}_j, t_0), v(\mathbf{x}_j, t_0)\}_{j=1}^{N_I}$ denoting the initial data, $\{t_B^j, \hat{u}(\mathbf{x}_{B_{1,2}}^j, t_B^j), \hat{v}(\mathbf{x}_{B_{1,2}}^j, t_B^j)\}_{j=1}^{N_B}$ standing for the periodic boundary data ($\mathbf{x}_{B_{1,2}}^j = (x_{1B_{1,2}}^j, x_{2B_{1,2}}^j)$ with $x_{iB_1}^j, x_{iB_2}^j$ representing the lower and upper bounds in i -axis), $\{\mathbf{x}_F^j, t_F^j\}_{j=1}^{N_F}$ representing the collocation points of PINNs $F(q, q_x, q_t, \dots) = F_u(q, q_x, q_t, \dots) + iF_v(q, q_x, q_t, \dots)$ within a spatio-temporal region $(\mathbf{x}, t) \in [-L, L]^2 \times (t_0, t_1]$. All of these sampling points are generated using a space filling Latin Hypercube Sampling strategy [36].

We would like to choose a multi-layer fully-connected neural network with some neurons per layer and a hyperbolic tangent activation function $\tanh(\cdot)$. We assume that $Q^j = (a_1^j, a_2^j, \dots, a_{m_j}^j)^T$ and $B^j = (b_1^j, b_2^j, \dots, b_{m_j}^j)^T$ denote the output and bias column vectors of the j -th layer, respectively, and $W^{j+1} = (w_{ks}^{j+1})_{m_{j+1} \times m_j}$ stands for the weight matrix of the j -th layer. In the input and output layers of neural networks, $Q^0 = (\mathbf{x}, t)^T = (x_1, x_2, t)^T$, $Q^{M+1} = (\hat{u}, \hat{v})^T$. The calculation in each hidden layer is shown as follows:

$$Q^{j+1} = \tanh(W^{j+1}A^j + B^{j+1}) \left(\tanh \left(\sum_{k=1}^{m_j} w_{1k}^{j+1} a_k^j + b_1^{j+1} \right), \dots, \tanh \left(\sum_{k=1}^{m_j} w_{m_{j+1}k}^{j+1} a_k^j + b_{m_{j+1}}^{j+1} \right) \right)^T. \tag{5}$$

The real and imaginary parts of solution, $u(\mathbf{x}, t)$ and $v(\mathbf{x}, t)$, are approximated by the two outputs, \hat{u} and \hat{v} , of one neural network, respectively (see Fig. 1).

In the following, we consider the data-driven rational solitons of the (2+1)-dimensional KP-I equation and spin-NLS equation via the deep neural networks learning.

2.2 Data-driven rational solitons of the (2+1)-D KP-I equation

In this part, we would like to consider the data-driven rational solitons of (2+1)-dimensional KP-I equation [37]

$$(q_t + 6qq_x + q_{xxx})_x - 3q_{yy} = 0, \tag{6}$$

which can be used to describe the propagation of long ion-acoustic waves with the small amplitude in plasmas [37], and the capillary gravitational waves on a liquid surface [38].

For the general evolutionary problem, we just use the initial loss (TL_I) and equation loss (TL_F). We choose the first-order rational soliton (also called the lump solution) of KP-I equation [39] as the initial data-set:

$$q(x, y, t) = \frac{F(x, y, t)}{G(x, y, t)}, \tag{7}$$

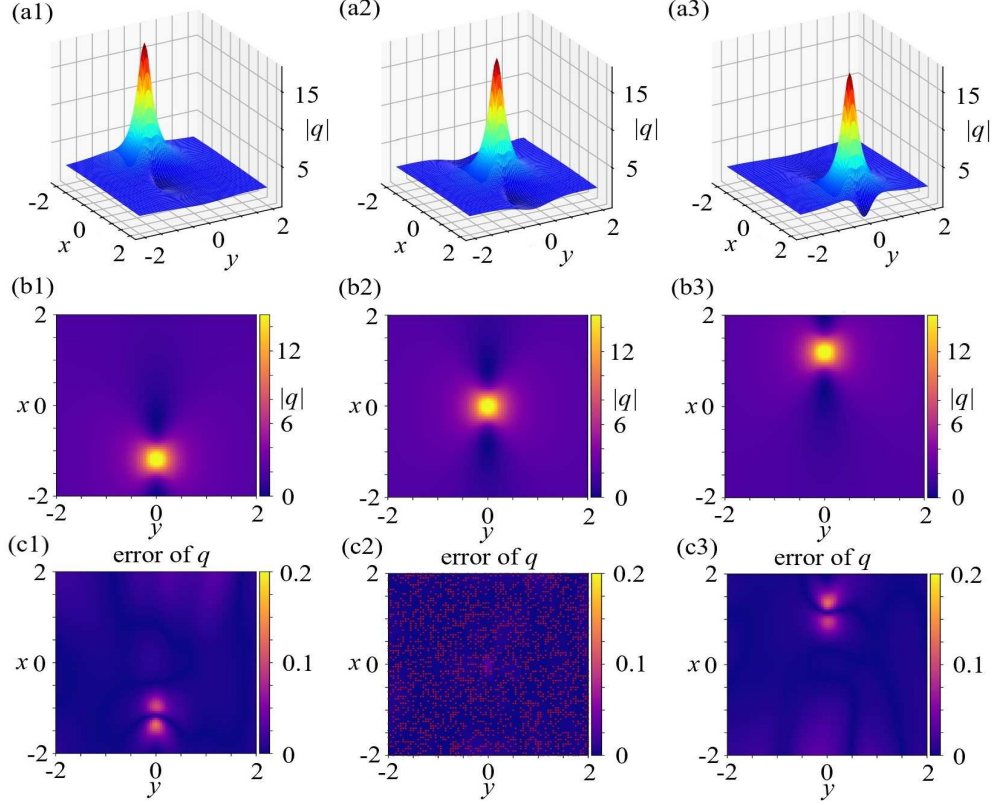


Figure 2: Data-driven rational soliton (7) of the KP-I equation (6). (a1-a3) the approximated solutions at $t = -0.05, 0, 0.05$. (b1-b3) density profiles of the approximated solutions at $t = -0.05, 0, 0.05$. (c1-c3) The absolute errors of the approximated solutions at $t = -0.05, 0, 0.05$. The relative L^2 -norm errors of $q(x, t)$, $u(x, t)$ and $v(x, t)$, respectively, are $2.878 \cdot 10^{-3}$, $2.878 \cdot 10^{-3}$, 0 . The training time is 1910.19s. The red dots in (c2) denote all sampling points of initial data set.

where

$$\begin{aligned}
 F(x, y, t) = & 256y^2x^2 + 512y^4 + 320y^2 + 512a^4y^4 - 12288y^2tx + 147456y^2t^2 + 32x^4 + 110592x^2t^2 \\
 & + 10616832t^4 - 1769472t^3x + 2304xt - 48x^2 - 27648t^2 - 3072x^3t + 18, \\
 G(x, y, t) = & (4x^2 + 16y^2 - 192xt + 2304t^2 + 1)^2.
 \end{aligned} \tag{8}$$

The rational soliton decays more slowly than the usual solitons with exponential decline [41].

We here choose $(x, y, t) \in [-2, 2] \times [-2, 2] \times [-0.05, 0.05]$ as the training domain. The 2,000 sample points ($N_I = 2,000$) are selected in $(x, y) \in [-2, 2] \times [-2, 2]$ for the initial data set, and 5,000 sample points ($N_S = 5,000$) are selected in the solution region $(x, y, t) \in [-2, 2] \times [-2, 2] \times [-0.05, 0.05]$ by Latin Hypercube Sampling strategy [36]. Notice that we here consider the free boundary conditions. We use a 6-layer fully connected neural network with 40 neurons per layer and a hyperbolic tangent activation function to approximate the solution $q(x, y, t)$. 10,000 steps Adam and 20,000 steps L-BFGS optimizations [40] are used in the training processes. Notice that in each step of the L-BFGS optimization, the program is stopped at $|\text{loss}(n) - \text{loss}(n-1)| / \max(|\text{loss}(n)|, |\text{loss}(n-1)|, 1) < 1.0 \times \text{np.finfo(float).eps}$,

Figs. 2(a1-a3, b1-b3) show that the approximated solution is shifting at the same speed along the x -

axis. Figs. 2(c1-c3) display that the PINN method can simulate rational soliton in the high-dimensional condition. The relative \mathbb{L}^2 -norm errors of $q(x, t)$, $u(x, t)$ and $v(x, t)$ are $2.878 \cdot 10^{-3}$, $2.878 \cdot 10^{-3}$, 0, respectively. The learning times is 1910.19s by using a Lenovo notebook with a 2.6GHz six-cores, i7 processor and a RTX2060 graphics processor.

2.3 Data-driven rational solitons of the (2+1)-D spin-NLS equation

In this subsection, we will consider the rational solitons of the (2+1)-dimensional spin-nonlinear Schrödinger (spin-NLS) equation:

$$iq_t + \alpha_1 q_{xx} + \alpha_2 q_{yy} + \alpha_3 q_{xy} - \alpha_4 |q|^2 q = 0, \quad (9)$$

where $q = q(x, y, t)$ denotes the complex envelope field, and the four real free parameters $\alpha_1, \alpha_2, \alpha_3$ and α_4 . Let $\xi = x + ky$, Eq. (9) can be transformed into the (1+1)-dimensional NLS equation:

$$iq_t + (\alpha_1 + \alpha_2 k^2 + \alpha_3 k) q_{\xi\xi} - \alpha_4 |q|^2 q = 0. \quad (10)$$

In the following, we will consider the first- and second-order rational solitons of Eq. (9).

2.3.1 Data-driven first-order W-shaped rational solitons

The first-order W-shaped rational soliton of Eq. (9) can be obtained by Darboux transform [42]:

$$q(x, y, t) = \left(\frac{4(1 - 2i\alpha_4 t)}{4k^2 y^2 + 4\alpha_4^2 t^2 + 8kxy + 4x^2 + 1} - 1 \right) e^{-i\alpha_4 t}, \quad k = -\frac{\alpha_3 \mp \sqrt{\alpha_3^2 - 4\alpha_2(\alpha_1 + \frac{1}{2}\alpha_4)}}{2\alpha_2}. \quad (11)$$

We use a 6-layer fully connected neural network with 40 neurons per layer and hyperbolic tangent activation function to approximate the first-order rational soliton (11) of Eq. (9). In order to ensure the accuracy of initial data, 1,000 initial sampling points ($N_I = 1,000$) are randomly chosen in $(x, y) \in [-10, 10] \times [-10, 10]$ at $t = 0$ and $\alpha_1 = 0.4$, $\alpha_2 = 1$, $\alpha_3 = -1$, $\alpha_4 = -2$ from the rational soliton (11). And 5,000 training sampling points ($N_S = 5,000$) are chosen in $(x, y, t) \in [-10, 10] \times [-10, 10] \times [-5, 5]$ by Latin Hypercube Sampling strategy [36].

Fig. 3 exhibits the approximated solutions and absolute errors at $t = 0, 1, 5$. The relative \mathbb{L}^2 -norm errors of $q(x, t)$, $u(x, t)$ and $v(x, t)$ are $2.449 \cdot 10^{-2}$, $1.940 \cdot 10^{-1}$, and $2.238 \cdot 10^{-1}$, respectively. In particular, it follows from Figs 3(a1-a3) that when the time increases from 0 to 5, the highest amplitude of the W-shaped rational soliton gradually decreases, and approaches the constant 1, that is, the W-shaped rational soliton finally degenerates the plane wave.

2.3.2 Data-driven second-order W-shaped rational solitons

The second-order rational solitons of (9) can be obtained [42]

$$q(x, y, t) = \left(1 + \frac{G_{21} - i\alpha_4 G_{22} t}{H_2} \right) e^{-i\alpha_4 t}, \quad (12)$$

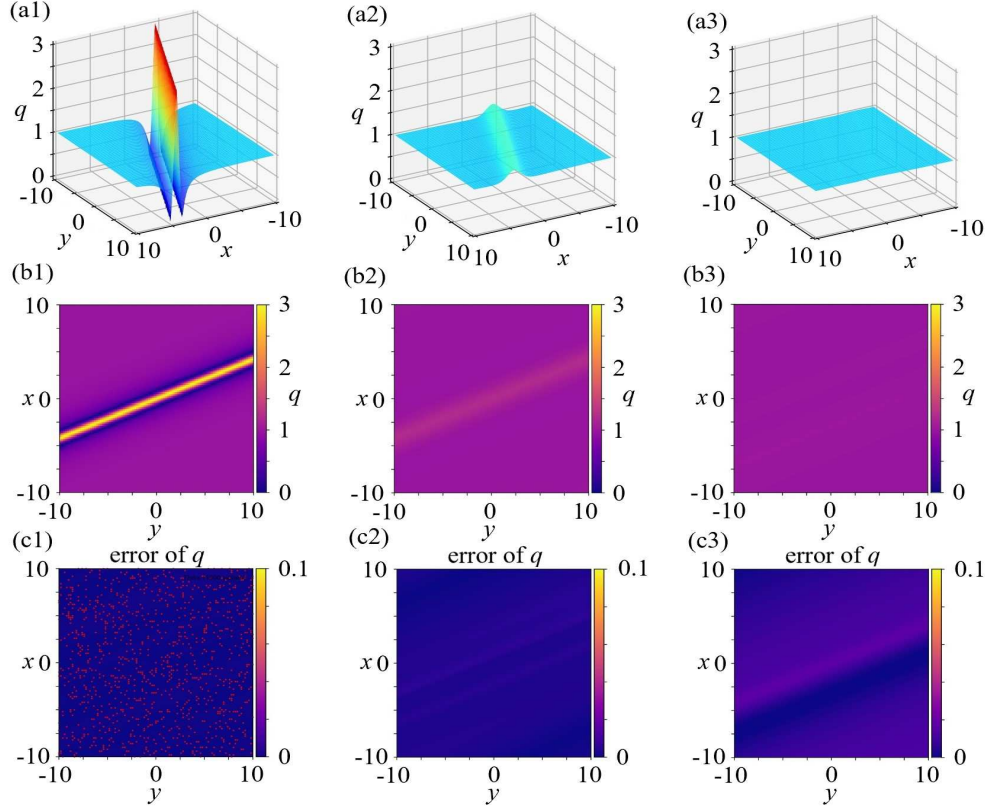


Figure 3: Data-driven 1-order rational soliton (11) of the spin-NLS equation (9). (a1-a3) The neural network solutions at $t = 0, 1, 5$, (b1-b3) the density profiles of the neural network solutions at $t = 0, 1, 5$, (c1-c3) the absolute errors of the neural network solutions at $t = 0, 1, 5$. The red dots in (c1) represent all initial sampling points. The relative \mathbb{L}^2 -norm errors of $q(x, t)$, $u(x, t)$ and $v(x, t)$, respectively, are $2.449 \cdot 10^{-2}$, $1.940 \cdot 10^{-1}$, $2.238 \cdot 10^{-1}$. The training time is 2115.12s.

where

$$\begin{aligned}
G_{21} &= -192k^4y^4 - 1152k^2\alpha_4^2t^2y^2 - 960\alpha_4^4t^4 - 768k^3xy^3 - 2304k\alpha_4^2t^2xy - 1152k^2x^2y^2 \\
&\quad - 1152\alpha_4^2t^2x^2 - 768kx^3y - 288k^2y^2 - 864\alpha_4^2t^2 - 192x^4 - 576kxy - 288x^2 + 36, \\
G_{22} &= -384k^4y^4 - 768k^2\alpha_4^2t^2y^2 - 384\alpha_4^4t^4 - 1536k^3xy^3 - 1536k\alpha_4^2t^2xy - 2304k^2x^2y^2 \\
&\quad - 768\alpha_4^2t^2x^2 - 1536kx^3y + 576k^2y^2 - 192\alpha_4^2t^2 - 384x^4 + 1152kxy + 576x^2 + 360, \\
H_2 &= 64k^6y^6 + 192k^4\alpha_4^2t^2y^4 + 192k^2\alpha_4^4t^4y^2 + 64t^6\alpha_4^6 + 384k^5xy^5 + 768k^3\alpha_4^2t^2xy^3 + 384k\alpha_4^4t^4xy \\
&\quad + 960k^4x^2y^4 + 1152k^2\alpha_4^2t^2x^2y^2 + 192\alpha_4^4t^4x^2 + 1280k^3x^3y^3 + 768k\alpha_4^2t^2x^3y + 48k^4y^4 + 108x^2 \\
&\quad - 288k^2\alpha_4^2t^2y^2 + 960k^2x^4y^2 + 432\alpha_4^4t^4 + 192\alpha_4^2t^2x^4 + 192k^3xy^3 - 576k\alpha_4^2t^2xy + 384kx^5y \\
&\quad + 288k^2x^2y^2 - 288\alpha_4^2t^2x^2 + 64x^6 + 192kx^3y + 108k^2y^2 + 396\alpha_4^2t^2 + 48x^4 + 108x^2 + 9,
\end{aligned} \tag{13}$$

where k still satisfies (11).

The solution (12) would be approximated by a 9-layer fully connected neural network with 20 neurons per layer. And the hyperbolic tangent activation function would be used to approximate the nonlinearity

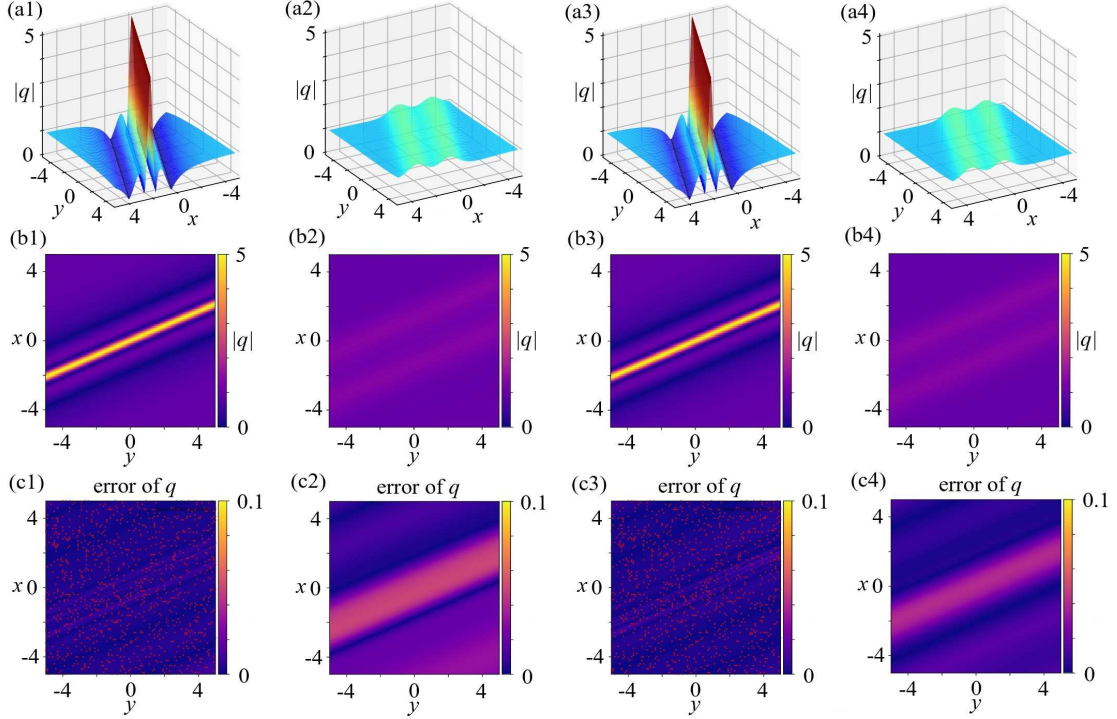


Figure 4: Data-driven 2-order rational soliton (12) of the (2+1)-D spin-NLS equation (9). (a1, a2) and (a3, a4) the approximated solutions arising from the unperturbed and perturbed (2%) training data related to the 2-order rational soliton initial data, respectively; (b1, b2, b3, b4) the corresponding density profiles of (a1, a2, a3, a4); (c1-c4) the absolute errors of the approximated solutions at $t = 0, 1$. The red dots in (c1, c3) represent all initial sampling points. The relative \mathbb{L}^2 -norm errors of $q(x, t)$, $u(x, t)$ and $v(x, t)$, respectively, are (unperturbed) $3.537 \cdot 10^{-2}$, $1.552 \cdot 10^{-1}$, $1.164 \cdot 10^{-1}$, (perturbed) $3.180 \cdot 10^{-2}$, $1.461 \cdot 10^{-1}$, $1.086 \cdot 10^{-1}$, . The training time of these two cases are 1326.92s and 1203.36s, respectively.

of (12). 1,000 initial sampling points ($N_I = 1,000$) are randomly chosen in $(x, y) \in [-5, 5] \times [-5, 5]$ at $t = 0$, and 5,000 training sampling points ($N_S = 5,000$) are chosen in $(x, y, t) \in [-5, 5] \times [-5, 5] \times [-2, 2]$ by Latin Hypercube Sampling strategy [36]. In this example, we assume $\alpha_1 = 0.4$, $\alpha_2 = 1$, $\alpha_3 = -1$, $\alpha_4 = -2$.

The training results are exhibited in Fig. 4. We divide the training processes into the unperturbed case (see, Figs. 4(a1, a2, b1, b2, c1, c2)) and perturbed case (see, Figs. 4(a3, a4, b3, b4, c3, c4)). The initial data set will be added 2% noise in the perturbed case. The relative \mathbb{L}^2 -norm errors of $q(x, t)$, real part $u(x, t)$ and imaginary part $v(x, t)$, respectively, are (unperturbed) $3.537 \cdot 10^{-2}$, $1.552 \cdot 10^{-1}$, $1.164 \cdot 10^{-1}$, (perturbed) $3.180 \cdot 10^{-2}$, $1.461 \cdot 10^{-1}$, $1.086 \cdot 10^{-1}$, . The training times of these two cases are 1326.92s and 1203.36s, respectively. Moreover, the same wave phenomena are also found similarly to the case of the data-driven first-order rational solitons in Sec. 2.3.1.

3 The inverse problems of higher-dimensional PDEs

In this section, we apply the PINNs deep learning method to solve the inverse problem (2) (i.e., discovering the parameters of the unknown equation $F(\mathbf{p}, q, q_x, q_t, \dots) = 0$). Firstly, we would like to briefly introduce

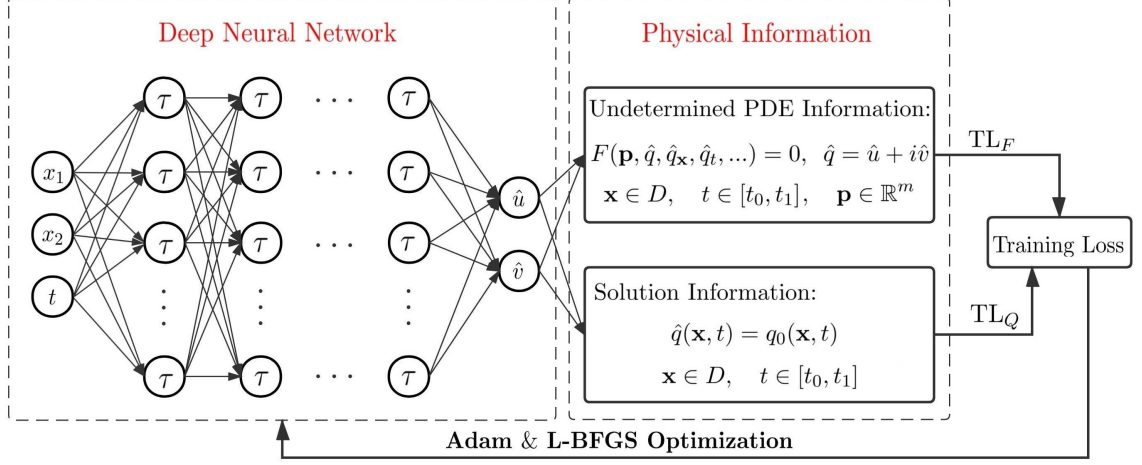


Figure 5: The PINN scheme solving the inverse problem (2), where \mathcal{T} denotes the activation function (e.g., $\mathcal{T} = \tanh(\cdot)$).

the PINN scheme for the inverse problem in the high-dimensional case (see Fig. 5). The loss function contains two parts: the solution loss (TL_Q) and undetermined-equation loss (TL_F). And a hyper-parameters λ_Q is added in the solution loss term (TL_Q) to balance the influence of solution loss and undetermined-equation loss during the optimization processes:

$$TL = \lambda_Q TL_Q + TL_F, \quad (14)$$

where

$$TL_Q = \frac{1}{N_Q} \sum_{j=1}^{N_Q} \left[\left(\hat{u}(\mathbf{x}_Q^j, t_Q^j) - u(\mathbf{x}_Q^j, t_Q^j) \right)^2 + \left(\hat{v}(\mathbf{x}_Q^j, t_Q^j) - v(\mathbf{x}_Q^j, t_Q^j) \right)^2 \right], \quad (15)$$

$$TL_F = \frac{1}{N_F} \sum_{j=1}^{N_F} \left(F_u^2(\mathbf{x}_F^j, t_F^j) + F_v^2(\mathbf{x}_F^j, t_F^j) \right).$$

As we did in the previous section, we divide TL_Q and TL_F into the real and imaginary parts, where $\{\mathbf{x}_Q^j, t_Q^j, u(\mathbf{x}_Q^j, t_Q^j), v(\mathbf{x}_Q^j, t_Q^j)\}_{j=1}^{N_Q}$ denote the solution data-set, and $\{\mathbf{x}_F^j, t_F^j\}_{j=1}^{N_F}$ represent the collocation points of PINN $F(q, q_x, q_t, \dots) = F_u(q, q_x, q_t, \dots) + iF_v(q, q_x, q_t, \dots)$ within a spatio-temporal region $(\mathbf{x}, t) \in [-L, L]^2 \times [t_0, t_1]$. This loss function will be trained by the Adam and L-BFGS optimization algorithm [40].

3.1 Data-driven parameter discovery for the (2+1)-D KP-I equation

In this part, we would like to consider the parameters discovery for the (2+1)-D KP-I equation through the PINNs deep learning method. We rewrite the original KP-I equation (6) as the extended form

$$(q_t + aqq_x + bq_{xxx} + cqq_{xxx})_x - q_{yy} = 0, \quad (16)$$

where a, b and c represent the unknown parameters, and the perturbation term qq_{xxx} is added in the equation to verify the validity of the algorithm.

Table 1: Data-driven parameter discovery of the KP-I equation (6). The training times of four cases are 2050.80s, 1963.42s, 1960.73s and 2305.53s.

| Case | a | error of a | b | error of b | c | error of c |
|-------------------|----------|-----------------------|---------|-----------------------|----------|-----------------------|
| Exact | -6 | 0 | 1 | 0 | 0 | 0 |
| Case 1 (no noise) | -6.03505 | 3.50×10^{-2} | 1.00871 | 8.71×10^{-3} | 0 | 0 |
| Case 1 (2% noise) | -5.94384 | 5.62×10^{-2} | 0.97842 | 2.17×10^{-2} | 0 | 0 |
| Case 2 (no noise) | -6.21099 | 2.11×10^{-1} | 1.05717 | 5.72×10^{-2} | -0.00071 | 7.13×10^{-4} |
| Case 2 (2% noise) | -5.88795 | 1.12×10^{-1} | 0.95398 | 4.60×10^{-2} | 0.00122 | 1.22×10^{-3} |

We will learn this equation in two cases. In the first case, the original KP-I equation will be learned without the perturbation term, i.e., $c = 0$. And in the second case, the KP-I equation will be learned with the above-mentioned perturbation term. Because the solution data of KP-I equation are all real, so we initialize the neural network with one output to represent the solution of KP-I equation. We use a 5-hidden layer with 40 neurons per layer to approximate the solution $q(x, y, t)$. The hyper-parameters λ_Q is set to 20 to increase the capability of solution approximation. 10,000 steps Adam and 50,000 steps L-BFGS optimization algorithm are used to train the model. The training data are generated by the rational soliton (7), which is an exact solution of (2+1)-D KP-I equation. The training domain is selected as $(x, y, t) \in [-2, 2] \times [-2, 2] \times [-0.05, 0.05]$, and 10,000 sampling points are randomly chosen from this area.

Table 1 shows the data-driven parameter discovery of the KP-I equation. The maximum relative error of undetermined parameters are 7.73×10^{-3} , 1.04×10^{-2} , 5.41×10^{-2} and 4.82×10^{-2} in above four cases. We can find that the PINN scheme can discover the unknown parameters successfully in the different cases. Fig. 6 displays the shapes and absolute errors of approximated rational solitons. In Figs. 6(a1-a3), the approximate solution propagates along the x -axis. And the relative \mathbb{L}^2 -norm errors of $q(x, y, t)$, are $1.91 \cdot 10^{-2}$, $1.48 \cdot 10^{-2}$, $1.87 \cdot 10^{-2}$ and $1.66 \cdot 10^{-2}$, respectively.

3.2 Data-driven parameter discovery for the coupled NLS-cmKdV equations

For the solution $q(x, y, t)$ of KP-I equation (6), the following transform [39]

$$q(x, y, t) = 2|r(x, y, t)|^2, \quad (17)$$

where $r(x, y, t)$ is a complex function of the variables x, y, t , can change the (2 + 1)-D KP-I equation (6) into the (1+1)-D NLS equation:

$$ir_y - r_{xx} - 2|r|^2r = 0, \quad (18)$$

and the (1+1)-D focusing complex mKdV (cmKdV) equation:

$$r_t + 4r_{xxx} + 24|r|^2r_x = 0. \quad (19)$$

In this subsection, we will consider the data-driven parameter discovery problem of the above-mentioned NLS and cmKdV equations via the data set of KP-I equation (i.e. we try to learn the unknown parameters

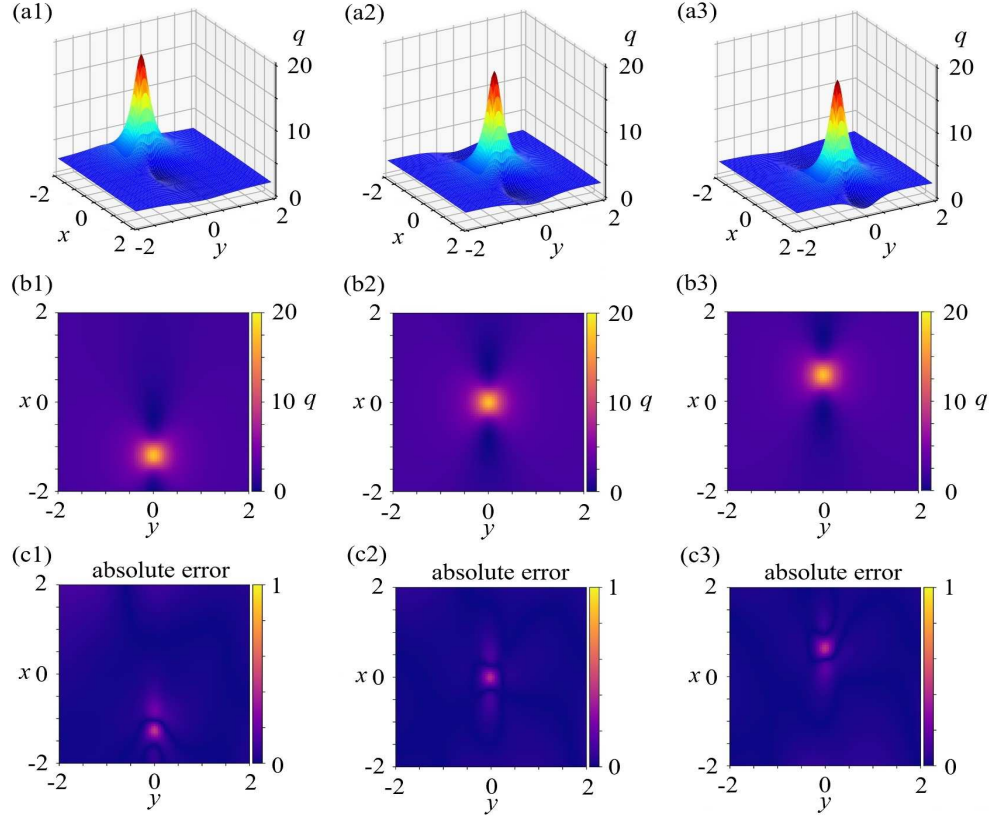


Figure 6: Data-driven inverse problem of the KP-I equation (6). (a1-a3) Three profiles of approximate solution at $t = -0.05, 0, 0.02$. (b1-b3) The density profiles of approximate solution at $t = -0.05, 0, 0.02$. (c1-c3) The absolute errors between approximate and exact solutions. The L^2 -norm errors of $q(x, y, t)$, are $1.91 \cdot 10^{-2}$, $1.48 \cdot 10^{-2}$, $1.87 \cdot 10^{-2}$ and $1.66 \cdot 10^{-2}$, respectively.

of NLS and cmKdV equations using the solution data set of KP-I equation). In order to achieve this goal, a transform loss (TL_T) will be added in the loss function [34]:

$$TL_T = \frac{1}{N_T} \sum_{j=1}^{N_T} \left[\hat{q}(\mathbf{x}_T^j, t_T^j) - 2 \left(\hat{u}(\mathbf{x}_T^j, t_T^j)^2 + \hat{v}(\mathbf{x}_T^j, t_T^j)^2 \right) \right]^2, \quad (20)$$

where $\{\mathbf{x}_T^j, t_T^j\}_{j=1}^{N_T}$ represent the collocation points of transform (17). In this example, a neural network with three outputs is used to approximate the q , u and v ($u = \text{Re}(r)$, $v = \text{Im}(r)$), respectively. They will share the same neural network parameters. We consider this problem by testing the data-driven parameter discovery of the coupled NLS-cmKdV equations from the following two cases:

- In case A, we assume that the unknown coupled NLS-cmKdV equations are:

$$\begin{cases} ir_y + ar_{xx} - 2|r|^2r + crr_x = 0, \\ r_t + br_{xxx} + 24|r|^2r_x + dr_x^2 = 0, \end{cases} \quad (21)$$

where the vector parameter $\mathbf{p} = (a, b, c, d)$ contains the four unknown parameters, and two perturbed quadratic terms are added in the original equations to test the robustness of this scheme.

Table 2: Data-driven parameter discovery of the coupled NLS-cmKdV equations (21, 22) via the transform (17): a, b, c, d , and their errors, as well as the training times.

| Case | a | b | c | d | |
|--------------|----------|----------|----------|----------|--|
| Exact of A | -1 | 4 | 0 | 0 | |
| A (no noise) | -1.00036 | 3.99994 | -0.00071 | -0.00077 | |
| A (2% noise) | -0.99935 | 3.99683 | -0.00014 | -0.00007 | |
| Exact of B | -2 | 24 | 0 | 0 | |
| B (no noise) | -1.97689 | 23.75477 | -0.00066 | -0.00093 | |
| B (2% noise) | -1.97442 | 23.73410 | -0.00049 | 0.00010 | |

| Case | error of a | error of b | error of c | error of d | time |
|--------------|-----------------------|-----------------------|-----------------------|-----------------------|----------|
| A (no noise) | 3.58×10^{-4} | 6.00×10^{-5} | 7.06×10^{-4} | 7.65×10^{-4} | 2146.21s |
| A (2% noise) | 6.51×10^{-4} | 3.17×10^{-3} | 1.38×10^{-4} | 6.80×10^{-5} | 2479.20s |
| B (no noise) | 2.31×10^{-2} | 2.46×10^{-1} | 6.33×10^{-4} | 9.27×10^{-4} | 2610.67s |
| B (2% noise) | 4.85×10^{-2} | 1.08×10^{-2} | 3.27×10^{-4} | 3.80×10^{-4} | 2624.10s |

- In case B, the unknown coupled NLS-cmKdV equations are taken as:

$$\begin{cases} ir_y - r_{xx} + a|r|^2r + crr_x = 0, \\ r_t + 4r_{xxx} + b|r|^2r_x + dr_x^2 = 0, \end{cases} \quad (22)$$

where the vector parameter $\mathbf{p} = (a, b, c, d)$ contains the four unknown parameters in the cubic nonlinear terms and perturbed quadratic terms.

A 6-layer fully connected network with 40 neurons per hidden layer will be used in Cases A and B. Both two cases will be trained by 10,000 steps and 20,000 steps L-BFGS optimization algorithm. 20,000 sampling points are randomly selected in $(x, y, t) \in [-2, 2] \times [-2, 2] \times [-0.05, 0.05]$. We still use the rational soliton (7) as the training data set.

Table 2 exhibits the training results of the coupled NLS-cmKdV equations. It is clear that the parameters can be learned well in Cases A and B. The maximum absolute errors in Cases A and B are 7.65×10^{-4} , 2.46×10^{-1} (without noise) and 3.17×10^{-3} , 4.85×10^{-2} (with 2% noise), respectively. The perturbed nonlinear terms have the effect on the discovery of nonlinear terms in the original equation, and the absolute values of coefficients of nonlinear terms become larger than high-order derivative terms. The \mathbb{L}^2 -norm errors of data set q are 4.59×10^{-3} (case A without noise), 3.29×10^{-3} (case A with 2% noise), 1.06×10^{-2} (case B without noise), 1.10×10^{-2} (case A with 2% noise), respectively. The FNN can approximate this data set really well. But the perturbed terms weaken the accuracies of the approximations.

3.3 Data-driven parameter discovery in the (2+1)-D spin-NLS equation

Here we would like to study the data-driven parameter discovery of the (2+1)-D spin-NLS equation (9). We will use the data-set generated by the 1-order and 2-order rational solitons given by Eqs. (11)-(12)

Table 3: Data-driven parameter discovery of the (2+1)-D spin-NLS equation (23): α_4 , c , and their errors, as well as training times.

| Case | α_4 | error of α_4 | c | error of c | time |
|--------------|------------|-----------------------|----------|-----------------------|----------|
| Exact of A | -2 | 0 | 0 | 0 | |
| A (no noise) | -1.99998 | 1.90×10^{-5} | -0.00047 | 4.65×10^{-4} | 1906.72s |
| A (2% noise) | -1.99964 | 3.59×10^{-4} | 0.00060 | 5.95×10^{-4} | 1839.14s |
| Exact of B | -2 | 0 | 0 | 0 | |
| B (no noise) | -1.99990 | 1.02×10^{-4} | 0.00121 | 1.21×10^{-3} | 2393.06s |
| B (2% noise) | -2.00037 | 3.72×10^{-4} | 0.00038 | 3.84×10^{-4} | 2910.89s |

to discover the original equation. We add a derivative-nonlinear perturbed term to verify the robustness of this scheme. The training equation (i.e., (2+1)-D generalized spin-NLS equation) can be written as:

$$iq_t + \alpha_1 q_{xx} + \alpha_2 q_{yy} + \alpha_3 q_{xy} - \alpha_4 |q|^2 q + cq q_x = 0, \quad (23)$$

where $\alpha_1 = 0.4$, $\alpha_2 = 1$, $\alpha_3 = -1$ are fixed, and the real-valued parameters α_4 and c will be learned and excluded during training processes. We set the initial values of α_4 , c to be 0 (Notice that the correct values of α_4 , c should be -2 and 0 , respectively). We use the data-set given by Eqs. (11)-(12) with $\alpha_4 = -2$ in Cases A and B, respectively. A 6-layer neural network with 40 neurons per layer is used to approximate the solution data. 10,000 sampling points are randomly selected in $(x, y, t) \in [-5, 5] \times [-5, 5] \times [-2, 2]$, and the residual points of TL_F are set to the same 10,000 sampling points.

We can find that the parameters α_4 , c of the previous nonlinear term and perturbed term can be discovered with the different data-set without noise or with a 2% noise (see Table 3). The relative L^2 norm of $q(x, y, t)$, real part $u(x, y, t)$ and imaginary part $v(x, y, t)$ are 5.04×10^{-2} , 4.16×10^{-2} , 4.40×10^{-2} for the case A without noise, 4.52×10^{-2} , 4.61×10^{-2} , 6.15×10^{-2} for the case A with 2% noise, 3.20×10^{-1} , 3.60×10^{-1} , 2.30×10^{-1} for the case B without noise, 7.85×10^{-1} , 7.88×10^{-1} , 3.58×10^{-1} for the case B with 2% noise. These result show that low frequency data-set are easier than high-frequency.

4 Conclusions and discussions

In conclusion, we have explored the data-driven rational solitons and parameter discovery of the (2+1)-D KP equation and (2+1)-D spin-NLS equation via the deep neural networks learning method. Especially, in the inverse problems, we use the PINNs to directly study the data-driven discovery parameters of the KP-I equation, and to investigate the parameters of NLS and cmKdV equations through the transform (17). Moreover, the data-driven parameter discovery of the (2+1)-D spin-NLS equation is investigated. The method can also be extended to other high-dimensional nonlinear wave equations.

Acknowledgments

This work is supported by the National Natural Science Foundation of China (Nos. 11925108 and 11731014).

References

- [1] A. Krizhevsky, I. Sutskever, and G.E. Hinton, Imagenet classification with deep convolutional neural networks, in: *Advances in Neural Information Processing Systems*, (2012) 1097-1105.
- [2] B.M. Lake, R. Salakhutdinov, and J.B. Tenenbaum, Human-level concept learning through probabilistic program induction, *Science* 350 (2015) 1332-1338.
- [3] B. Alipanahi, A. Delong, M.T. Weirauch, and B. J. Frey, Predicting the sequence specificities of DNA- and RNA-binding proteins by deep learning, *Nat. Biotechnol.* 33 (2015) 831-838.
- [4] I. Goodfellow, Y. Bengio, and A. Courville, *Deep learning* (MIT Press, 2016).
- [5] P. Larranaga, D. Atienza, J. Diaz-Rozo, A. Ogbechie, C. E. Puerto-Santana, and C. Bielza, *Industrial Applications of Machine Learning*, CRC Press (2019).
- [6] P. Johri, J. K. Verma, and S. Paul (ed.), *Applications of Machine Learning* (Springer, 2020).
- [7] K. Hornik, M. Stinchcombe, and H. White, Multilayer feedforward networks are universal approximators, *Neural Networks* 2 (1989) 359-366.
- [8] K. Hornik, Approximation capabilities of multilayer feedforward networks, *Neural Networks* 4 (1991) 251-257.
- [9] P. Allan, Approximation theory of the MLP model in neural networks, *Acta Numerica* 8 (1999) 143-195.
- [10] W. E, C. Ma, S. Wojtowytsch, and L. Wu, Towards a Mathematical Understanding of Neural Network-Based Machine Learning: what we know and what we don't, arXiv:2009.10713.
- [11] W. E, A proposal on machine learning via dynamical systems, *Commun. Math. Stat.* 5 (2017) 1-11.
- [12] R. DeVore, B. Hanin, and G. Petrova, Neural network approximation, *Acta Numerica* 30 (2021) 327-444.
- [13] Y. Zang, G. Bao, X. Ye, and H. Zhou, Weak adversarial networks for high-dimensional partial differential equations, *J. Comput. Phys.* 411 (2020) 109409.
- [14] J. Han, A. Jentzen, and W. E, Solving high-dimensional partial differential equations using deep learning, *PNAS* 115 (2018) 8505-8510.
- [15] C. Beck, W. E, and A. Jentzen, Machine learning approximation algorithms for high-dimensional fully nonlinear partial differential equations and second-order backward stochastic differential equations, *J. Nonlinear Sci.* 29 (2019) 1563-1619.
- [16] W. E, J. Han, and A. Jentzen, Deep learning-based numerical methods for high-dimensional parabolic partial differential equations and backward stochastic differential equations, *Commun. Math. Stat.* 5 (2017) 349-380.
- [17] J. Behler, Atom-centered symmetry functions for constructing high-dimensional neural network potentials, *J. Chem. Phys.* 134 (2011) 074106.
- [18] K. V. Jovan Jose, N. Artrith, and J. Behler, Construction of high-dimensional neural network potentials using environment dependent atom pairs, *J. Chem. Phys.* 136 (2012) 194111.
- [19] W. E and B. Yu, The Deep Ritz Method: A Deep Learning-Based Numerical Algorithm for Solving Variational Problems, *Commun. Math. Stat.* 6 (2018) 1-12.
- [20] M. Raissi, P. Perdikaris, and G. E. Karniadakis, Physics-informed neural networks: A deep learning framework for solving forward and inverse problems involving nonlinear partial differential equations, *J. Comput. Phys.* 378 (2019) 686.
- [21] S. Goswami, C. Anitescu, S. Chakraborty, and T. Rabczuk, Transfer learning enhanced physics informed neural network for phase-field modeling of fracture, *Theor. Appl. Fract. Mech.* 106 (2020) 102447.
- [22] A. D. Jagtap, K. Kawaguchi, and G. E. Karniadakis, Adaptive activation functions accelerate convergence in deep and physics-informed neural networks, *J. Comput. Phys.* 404 (2020) 109136.
- [23] X. Meng, Z. Li, D. Zhang, and G. E. Karniadakis, PPINN: Parareal physics-informed neural network for time-dependent PDEs, *J. Comput. Phys.* 370 (2020) 1132.
- [24] J. Sirignano and K. Spiliopoulos, DGM: A deep learning algorithm for solving partial differential equations, *J. Comput. Phys.* 375 (2018) 1339-1364.
- [25] Z. Long, Y. Lu, X. Ma, and B. Dong, PDE-Net: Learning PDEs from Data, *Proceedings of the 35th International Conference on Machine Learning*, PMLR 80 (2018) 3208-3216.

- [26] Z. Long, Y. Lu, and B. Dong, PDE-Net 2.0: Learning PDEs from data with a numeric-symbolic hybrid deep network, *J. Comput. Phys.* 399 (2019) 108925.
- [27] L. Lu, X. Meng, Z. Mao, and E. K. George, DeepXDE: A deep learning library for solving differential equations, *SIAM Rev.* 63 (2021) 208-228.
- [28] C. Michoski, M. Milosavljevic, T. Oliver, et al., Solving differential equations using deep neural networks, *Neurocomputing* 399 (2020) 193-212.
- [29] J. Pu, J. Li, and Y. Chen, Soliton, breather and rogue wave solutions for solving the nonlinear Schrödinger equation using a deep learning method with physical constraints, *Chin. Phys. B* 30 (2021) 060202.
- [30] Z. Zhou and Z. Yan, Solving forward and inverse problems of the logarithmic nonlinear Schrödinger equation with PT-symmetric harmonic potential via deep learning, *Phys. Lett. A* 387 (2021) 127010.
- [31] L. Wang and Z. Yan, Data-driven rogue waves and parameter discovery in the defocusing NLS equation with a potential using the PINN deep learning, *Phys. Lett. A* 404 (2021) 127408.
- [32] Z. Zhou and Z. Yan, Deep learning neural networks for the third-order nonlinear Schrödinger equation: Bright solitons, breathers, and rogue waves, *Commun. Theor. Phys.* 73 (2021) 105006.
- [33] L. Wang and Z. Yan, Data-driven peakon and periodic peakon travelling wave solutions of some nonlinear dispersive equations via deep learning, *Physica D* 428 (2021) 133037 (arXiv:2101.04371).
- [34] Z. Zhou, L. Wang, and Z. Yan, Data-driven discovery of Bäcklund transforms and soliton evolution equations via deep neural network learning schemes, arXiv:2111.09489.
- [35] M. Raissi, Deep hidden physics models: deep learning of nonlinear partial differential equations, *J. Mach. Learn. Res.* 19 (2018) 932-955.
- [36] M. Stein, Large sample properties of simulations using Latin hypercube sampling, *Technometrics* 29 (1987) 143-151.
- [37] B. B. Kadomtsev and V. I. Petviashvili, On the stability of solitary waves in weakly dispersive media, *Sov. Phys. Dokl.* 15 (1970) 539-541.
- [38] S. Zhdanov and B. Trubnikov, Soliton chains in a plasma with magnetic viscosity, *ZhETF Pis'ma v Redaktsiiu*, 39 (1984) 110-113.
- [39] X. Wen and Z. Yan, Higher-order rational solitons and rogue-like wave solutions of the (2+1)-dimensional nonlinear fluid mechanics equations, *Commun. Nonlinear Sci. Numer. Simulat.* 43 (2017) 311-329.
- [40] D. C. Liu, J. Nocedal, On the limited memory BFGS method for large scale optimization, *Math. Program.* 45 (1989) 503-528.
- [41] M.J. Ablowitz and P. A. Clarkson, *Soliton, Nonlinear Evolution Equations and Inverse Scattering* (Cambridge University Press, Cambridge, 1991).
- [42] B. Li and Y. Ma, Lax pair, Darboux transformation and Nth-order rogue wave solutions for a (2+1)-dimensional Heisenberg ferromagnetic spin chain equation, *Comput. Math. with Appl.* 77 (2019) 514-524.